View metadata, citation and similar papers at core.ac.uk

brought to you by CORE

provided by Purdue E-Pubs

Purdue University
Purdue e-Pubs

International Refrigeration and Air Conditioning Conference

School of Mechanical Engineering

2014

Using Surface Wettability to Impact the Frost Properties and Defrosting Effectiveness of a Metallic Heat Transfer Surface

Nicholas Truster
Dept. of Mechanical and Manufacturing Engineering, Miami University, Oxford, OH 45056, trustenl@miamioh.edu

Catherine Puleo
Dept. of Chemical, Paper, and Biomedical Engineering, Miami University, Oxford, OH 45056, puleoce@miamioh.edu

Edgar Caraballo
Dept. of Mechanical and Manufacturing Engineering, Miami University, Oxford, OH 45056, carabaej@miamioh.edu

Andrew Sommers
Dept. of Mechanical and Manufacturing Engineering, Miami University, Oxford, OH 45056, sommerad@miamioh.edu

Follow this and additional works at: http://docs.lib.purdue.edu/iracc

Truster, Nicholas; Puleo, Catherine; Caraballo, Edgar; and Sommers, Andrew, "Using Surface Wettability to Impact the Frost Properties and Defrosting Effectiveness of a Metallic Heat Transfer Surface" (2014). *International Refrigeration and Air Conditioning Conference*. Paper 1476.
http://docs.lib.purdue.edu/iracc/1476

This document has been made available through Purdue e-Pubs, a service of the Purdue University Libraries. Please contact epubs@purdue.edu for additional information.
Complete proceedings may be acquired in print and on CD-ROM directly from the Ray W. Herrick Laboratories at https://engineering.purdue.edu/Herrick/Events/orderlit.html

Using Surface Wettability to Impact the Frost Properties and Defrosting Effectiveness of a Metallic Heat Transfer Surface

Nicholas L. TRUSTER[1], Catherine E. PULEO[2], Edgar J. CARABALLO[1], Andrew D. SOMMERS[1,*]

[1] Dept. of Mechanical and Manufacturing Engineering, Miami University, Oxford, OH 45056 USA
Phone: (513) 529-0718, Fax: (513) 529-0717, E-mail: sommerad@miamioh.edu

[2] Dept. of Chemical, Paper, and Biomedical Engineering, Miami University, Oxford, OH 45056 USA
Phone: (513) 529-0760

* Corresponding Author

ABSTRACT

In this work, the properties of a growing frost layer were analyzed for surfaces of varying wettability to determine the effect that the surface energy has on the frost mass, thickness, and density. Both patterned and non-patterned surfaces were explored. To date, three surfaces have been fabricated and tested— an uncoated, untreated aluminum plate (Sample 1), a plate coated with a super-hydrophobic coating (Sample 2), and a plate containing a triangular surface wettability pattern (Sample 3). For these experiments, the frost layer was grown for a three-hour period inside a Plexiglas environmental test chamber where the relative humidity was held constant during the experiment at either 60% or 80%, and the surface temperature of the plate was fixed using a thermoelectric cooler (TEC). The temperature of the ambient air inside the Plexiglas enclosure was also recorded to ensure that it remained constant for the duration of the experiment. The TEC unit was placed on an electronic balance inside the test chamber which permitted the continuous recording of frost mass during both the frosting and defrosting portions of the experiment. Images of the frost layer were also taken using a CCD camera mounted directly overhead and parallel to the face of the plate. Frost thickness was then determined from these images by pixel counting methods. Our data show that the hydrophobic surface coating on Sample 2 resulted in a decrease of the frost density by nearly 100% as compared to the uncoated, baseline surface (Sample 1). This was largely because the baseline surface accumulated 60-90% more frost mass than the hydrophobic surface during the same allotted time period. The thickness of the frost layer was also slightly smaller on the baseline surface than the hydrophobic surface. The overall aim of this work is to study the effects that micro-structural roughness and surface anisotropy have on a growing frost layer and to better understand the defrosting process on functionalized heat transfer surfaces.

1. INTRODUCTION

The study and development of micro-structured, anisotropic surfaces for use in the refrigeration, air-conditioning, aerospace, and automotive industries represents a valuable step in advancing our current understanding and design of more energy efficient systems and structures. For example, in refrigeration systems, heat exchanger fin spacing is often quite large to mitigate frost blockage, and thus the convective heat transfer coefficient is typically low. Because of the requirement for periodic defrosting, refrigerator evaporators tend to be rather inefficient due to this periodic downtime. In air conditioning systems, water that does not drain off the evaporator eventually goes back into the air and must therefore be condensed again which increases the latent load of the system. Furthermore, water retention on the heat exchanger increases fan power requirements due to the increased drag and can result in "condensate carryover" into the occupied space. Thus, the HVAC&R industry stands to benefit significantly from this research; however, it is expected that this research would also benefit the aerospace and automotive industries where this technique might be used to mitigate surface drag, improve wing de-icing, etc. It is also important to note that methods currently exist for creating water repellent and frost tolerant surfaces; however, these approaches typically rely upon chemical coatings which break down over time due to the thermal cycling and large temperature gradients experienced in these systems.

Over the years, numerous frost studies have been published. Östin and Andersson (1991) concluded that the plate surface temperature and the air relative humidity both affect frost thickness; whereas, the density of the frost largely depends on the air velocity and to a lesser extent on the relative humidity. Density, however, was independent of surface

temperature. Similarly, the mass deposition rate of the frost was shown to have considerable dependence upon the relative humidity and air velocity. Östin and Andersson (1991) also examined the contribution of the mass flux of condensed vapor to frost density and frost thickness and found that the condensing water vapor contributes nearly equally to the increase of frost density and frost thickness. Rite and Crawford (1991) examined the impact that various environmental parameters have on the frost rate of an evaporator and found that a theoretical frost deposition rate based on measured upstream and downstream relative humidities was reasonably accurate. They also observed that the average frosting rate flux was essentially the same after 10 hours as it was after 5 hours, whereas Senshu (1990) had suggested that the frosting rate decreased with increasing air velocity. Other relevant works include Hayashi et al. (1977) who derived a correlation to calculate the frost density, and Brian et al. (1970) who developed a correlation for calculating the effective thermal conductivity of the frost layer based on the mean frost surface temperature and the average frost density. Other published methods for predicting frost properties on conventional surfaces (esp. thermal conductivity) include Yang and Lee (2004), Yang et al. (2004), Yonko and Sepsy (1967), and Lee et al. (1997).

Using the frost property models of Hayashi et al. (1977) and Brian et al. (1970), Cheng and Cheng (2001) proposed a theoretical model for predicting the frost growth rate on a flat plate. Assumptions inherent to this model included uniform frost density throughout the frost layer at any instant, orthogonal growth of the frost layer relative to the plate surface, uniform frost thickness, and constant heat and mass transfer coefficients (h and h_m) on the frost surface. Comparisons were made with other existing theoretical models by Jones and Parker (1975) and Sherif et al. (1993). Cheng and Wu (2003) examined frost formation on a flat plate subjected to atmospheric air flow in an open-loop wind tunnel using a CCD camera. They distinguished between three different time periods in the formation of frost as was done previously by Hayashi et al. (1977) and called them the *crystal growth period*, *frost layer growth period*, and *full growth period*, respectively. More recent models for the prediction of the frost growth rate use supersaturated water vapor at the frost surface instead of saturated vapor such as Na and Webb (2004a, 2004b). Other relevant models of frost growth and densification include Schneider (1978), Tao et al. (1993), White and Cremers (1981), Yun et al. (2002), Inaba and Imai (1996), LeGall and Grillot (1997), Cheng and Cheng (2001), Cheng and Wu (2003) and Ogawa et al. (1993).

Although many studies have been performed to model frost properties, relatively few papers were found which specifically examined the effect of surface wettability on the growing frost layer. In a paper by Shin et al. (2003), three different surfaces having dynamic contact angles (DCA) of 23°, 55°, and 88° were installed in a wind tunnel and exposed to a humid air flow. They found that during the initial period of frost formation, the shape of the micro droplets depended upon the surface energy and the process of frost growth was affected by the DCA. High DCA surfaces showed the presence of irregular and rough crystals during the initial period of frost deposition, which resulted in high frost thickness and low frost density. By comparison, low DCA surfaces showed uniform and regular crystals resulting in low frost thickness and high density. This suggests that the growth of crystals is strictly controlled by surface energy during the early stages of frost growth. However, when the frost thickness was observed to reach a certain level, frost formation tended to be influenced instead by the environmental conditions rather than by the surface characteristics. Another recent study by Kulinich et al. (2011) showed that super-hydrophobic surfaces are not always ice-repellent and that the ice-repellent properties of super-hydrophobic materials can deteriorate during icing/deicing cycles due to damage to the surface asperities. They also showed that the anti-icing efficiency of super-hydrophobic surfaces is significantly lower in a humid atmosphere due to increased ice adhesion strength.

2. EXPERIMENTAL METHOD

2.1 Experimental Methodology / Data Collection

In this study, two different types of frost experiments were performed— i.e. one concerned principally with the properties of the growing frost layer (i.e. Normal Frost Growth NFG) and the other concerned with the defrosting performance of the surface and issues related to multiple frost/defrost events (i.e. Cycling Tests CT). During these tests, the surface temperature was prescribed using a thermoelectric cooler (TEC). The air temperature and relative humidity were also recorded during each test and held constant using cool mist humidification. Table 1 below shows a matrix of the operating conditions associated with each experiment. Normal Frost Growth (NFG) experiments were three hours in duration followed by ten minutes of defrosting. Cycling tests (CT) lasted three hours and fifteen minutes and consisted of three one-hour frost growth periods followed by five minutes of defrosting after each period. Thus, these tests consisted of three separate frosting/defrosting events (i.e. three cycles). The test samples were constructed from aluminum alloy 5052 polished on one side to a brushed finish. The plates were affixed to the

TEC stage using thermal paste and four Nylon screws with Teflon spacers to minimize water retention and thermal losses from the surface. The test surfaces all had the same dimensions and were approximately 99.5 mm × 80.2 mm × 3.4 mm in size. The total surface area of the plates was 7979.9 mm^2. Details about the various plates and their differences in wettability can be found in Table 2. Some of these surfaces were engineered with a surface tension gradient to help facilitate the movement of water to preferred locations on the surface.

Table 1: Matrix of experimental test conditions

Test Condition A 60% RH 16.0V or -3ºC	**Test Condition B** 60% RH 18.6V or -6ºC	**Test Condition C** 60% RH 22.0V or -9ºC
Test Condition D 80% RH 16.0V or -3ºC	**Test Condition E** 80% RH 18.6V or -6ºC	**Test Condition F** 80% RH 22.0V or -9ºC

Table 2: Matrix of heat transfer test surfaces

No.	Material	Gradient	Surface Features	Method
1	Al	N	None	--
2	Al	N	Hydrophobic Coating (NeverWet™ spray-on coating)	Spray Coating
3	Al	Y	Hydrophobic / Hydrophilic Wedges (with SAM coating)	Metal Deposition
4	Al	Y	Laser Etched Radial Design (planned)	Laser Machining

2.2 Environmental Test Chamber

All experiments were performed in an environmental test chamber. To isolate the environmental conditions, a Plexiglas enclosure with a hinged, sealable lid was placed around the equipment as shown in Figs. 1 and 2 below. This Plexiglas enclosure had the dimensions 400.1mm × 257.2mm × 285.8mm. A Plexiglas partition was inserted vertically inside the box to create a front and rear chamber inside of the enclosure, thereby permitting higher relative humidities to be achieved near the sample and to help maintain a constant air temperature inside the front chamber. This partition was secured so as not to affect the balance. An ultrasonic cool mist humidifier was used to maintain the relative humidity inside the test chamber to within ±2.5% of the desired value, and the air temperature inside the enclosure was typically held constant to within ±0.5ºC as shown in Fig. 3. An OMEGA OM-73 temperature/relative humidity data logger was used to record the environmental conditions during each test (±2% RH accuracy).

A GP5202 Sartorius balance connected to a laptop through a small hole in the rear partition of the Plexiglas enclosure was used for the real-time measurement of the frost mass. The frost mass was sampled and recorded at a frequency of approximately once every 0.2 seconds. A CP-061 Peltier thermoelectric cold plate cooler placed atop the balance and connected to a DC power supply was used to cool the surface. To accurately measure the frost growth, frost was only permitted to grow on the face of the test plate. To ensure frost growth only occurred on the test plate, multiple layers of insulation tape were placed around the edges of the thermoelectric cooler (TEC). A drip guard (isolated from the rest of the equipment) was placed underneath the face of the thermoelectric cooler to prevent any condensate and/or melted frost from draining onto the balance and affecting the mass measurement. The test plate was secured to the face of the thermoelectric cooler with Nylon screws and spacers to prevent frost build-up on the head of the screws. Thermal paste was used to secure the test plate to the face of the thermoelectric cooler and to help minimize the contact resistance between the plate and the stage. Four T-type thermocouples were used to measure the plate and stage temperatures (two on each side) during an experiment. The stage temperature was determined using two thermocouples affixed directly to the TEC surface by epoxy. The test plate temperature was determined using two thermocouples inserted into small holes drilled into the side of the test plates (one on each side). The depth of the holes was approx. 6-8 mm. Thermal paste was applied to the thermocouple junction before insertion, and epoxy was used to hold the thermocouple securely in place.

At the start of each test, the desired voltage was set for the TEC, and a thin plastic sheet was applied to the test surface to prevent condensation and/or frosting on the surface before the desired surface temperature was reached. Once the set-point temperature was reached, the plastic sheet was removed and the frost growth period was started. All tests were performed at constant voltage to the TEC. Defrosting was initiated by turning 'OFF' the power to the TEC and allowing the stage to warm up to room temperature and melt the frost. A Pixelink PL-B871CU CCD camera (1392 x 1040 resolution; 10 fps) placed on top of the Plexiglas enclosure (parallel to the face of the test plate) was used to record pictures of the frost thickness every 5 minutes during the frost growth period and every 30 seconds during defrosting. At the start of every experiment, a calibration image was taken. Pixel counting techniques were then used to determine the thickness of the frost layer as a function of time. When coupled with the mass measurement, the average density of the frost layer could also be determined as a function of time.

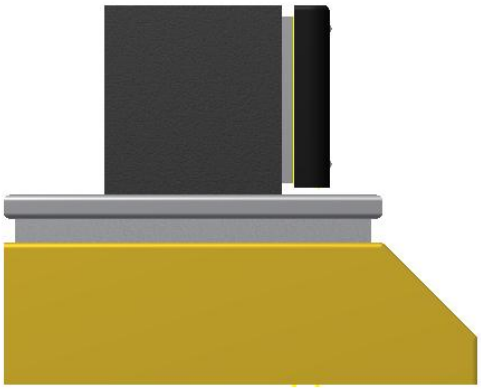

Figure 1: Thermoelectric cooler with insulation tape on the Sartorius balance

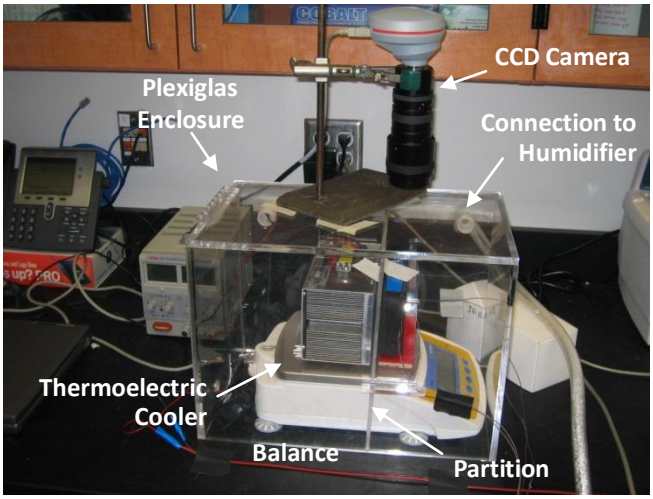

Figure 2: Experimental Setup Information

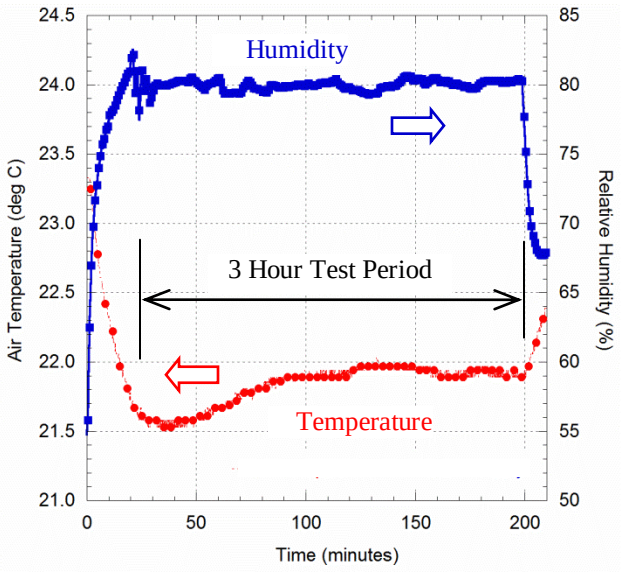

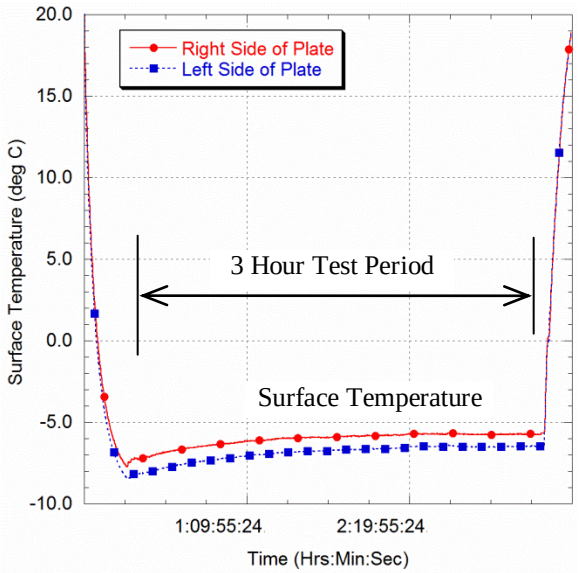

Figure 3: Environmental conditions during a typical NFG baseline test (80% RH, 18.6V TEC)

3. RESULTS AND DISCUSSION

As shown in the experiments, surface energy (i.e. wettability) can have a significant effect on the properties of a growing frost layer as well as water removal efficiency during a defrosting event. Surface energy is most commonly quantified by measuring the contact angle that a droplet makes with a surface. Hydrophilicity (i.e. higher surface energy) is indicated by smaller contact angles, and hydrophobicity (i.e. lower surface energy) is indicated by high contact angles. In this work, a ramé-hart contact angle goniometer was used to measure the static contact angle formed by water droplets injected on the test samples using the sessile drop method (see Table 3). As shown in this table, Sample 2 possessed a static contact angle of more than 150° which classifies the surface as being "super-hydrophobic." This contact angle was more than 50° higher than the baseline surface (i.e. Sample 1). It is also important to note that while there was an apparent decrease in the static contact angle following testing, the surface largely retained its hydrophobicity. This is noteworthy since other researchers have reported that super-hydrophobic materials may deteriorate in ice-repellency following multiple icing/deicing cycles (Kulinich, 2011). In all cases, more than 25 measurements were recorded in arriving at these average values. Figure 4 shows representative images of water droplets on both the baseline surface and the hydrophobic surface (i.e. Samples 1 and 2).

3.1 Normal Frost Growth Experiments

Experiments were first performed on Sample 1 (baseline surface) for the conditions shown in Table 1 to check the accuracy of the experimental set-up and data reduction methodology. The overall results were in good agreement with previous research (Hoke et al., 2004; Lee et al., 1997). In Figs. 5 and 6, the transient behavior of the growing frost layer is shown as a function of the environmental conditions. In Fig. 5, the frost thickness is shown first as a function of the surface temperature (holding RH constant) and then as a function of the air relative humidity (holding surface temperature constant). As seen in the figure, the frost thickness scaled inversely with the surface temperature (see Fig. 5a) but directly with the relative humidity (see Fig. 5b). This was predicted by Hayashi (1977) who classified frost formation type with surface temperature and found that thinner, denser frost layers formed on warmer surfaces and thicker frost layers were formed on colder surfaces. In another work (Lee et al., 1997), the influence of relative humidity was examined, and the thickness of the frost layer was shown to increase with humidity. Thus as might be expected, the frost thickness was greatest on the –9°C baseline surface (versus the –3°C surface) and on the surface exposed to 80% RH (versus 60% RH). In both cases, these differences did not start to manifest themselves until after approximately 30 min of frosting. The maximum observed difference in frost thickness was approx. 0.5 mm.

As seen in Fig. 6, the mass of frost on the baseline surface was also higher at 80% RH than at 60% RH as might be expected. This is consistent with the higher mass transfer that would occur at elevated air moisture levels. Also noteworthy is the fact that while the frost mass increased linearly with time, the frost thickness increased nonlinearly with time. This suggests that the condensing water vapor contributed both to increasing the frost density as well as to increasing the frost thickness— something that has been observed by others (Östin and Andersson, 1991).

Table 3: Contact angles on test plates

No.	Surface	Contact Angle
1	Baseline Surface	98.4º (n > 25)
2	Hydrophobic Surface (after testing)	151.5º (n > 25)
	Hydrophobic Surface (not used in testing)*	156.5° (n > 25)

*For comparison only. Small decrease in CA was observed.

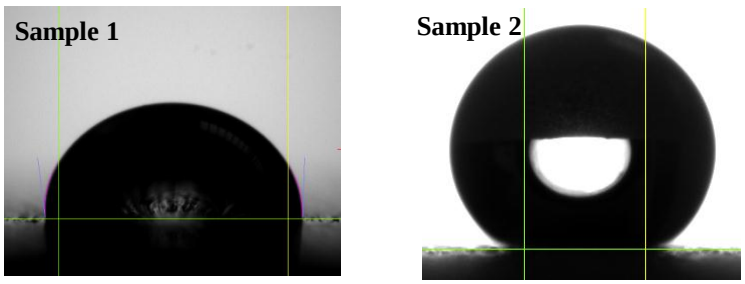

Figure 4: Water droplet contact angles on Samples 1 and 2 (typical)

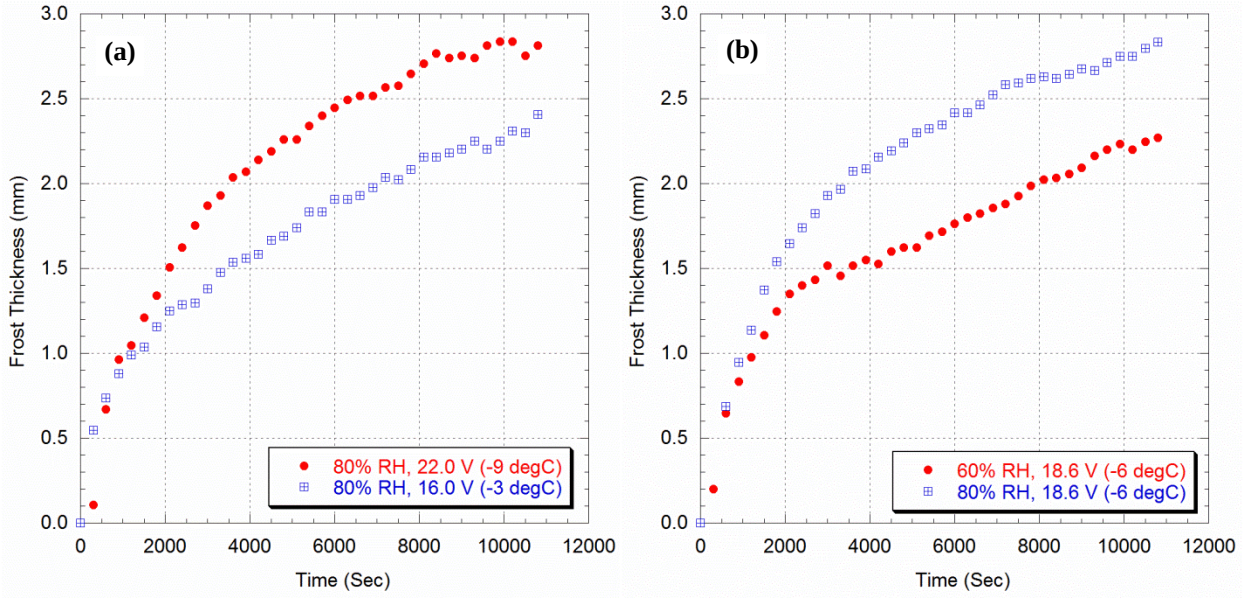

Figure 5: Effect of surface temperature and relative humidity on frost thickness for Sample 1

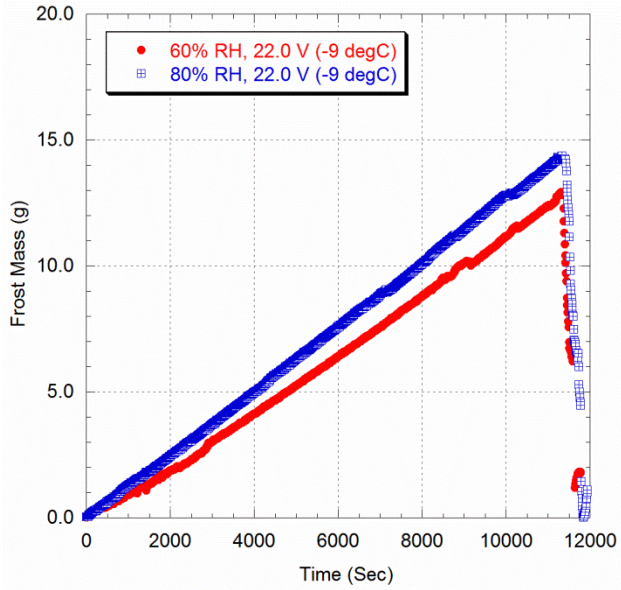

Figure 6: Effect of relative humidity on the deposited frost mass for Sample 1

Next, the tests were performed on the hydrophobic surface (Sample 2) and compared against the baseline surface (Sample 1). Representative images of the growing frost layer can be seen in Fig. 7. These images were both taken at approximately 150 minutes into the experiment under the same environmental conditions (80% RH, 22.0V TEC). Differences in the frost thickness can be seen by comparing the height of the frost layer to the nylon screw at the left. Markings were made on the screw corresponding to 1 mm intervals. Thus, it can be seen that the frost thickness on the baseline surface was less than 3 mm while the frost layer on Sample 2 was ≥ 3 mm thick. (Note: Due to small differences in camera orientation each time, the scaling in these two images may be slightly different.)

Fig. 8 shows the differences in the properties of the frost layer between the baseline surface and the hydrophobic surface over the three-hour testing period. The frost mass was smaller on the hydrophobic surface while at the same time the frost thickness was larger. As a result, the overall density of the frost layer on the hydrophobic (low energy) surface was smaller than the frost density on the baseline surface (see Fig. 8.). As a consequence, the frost

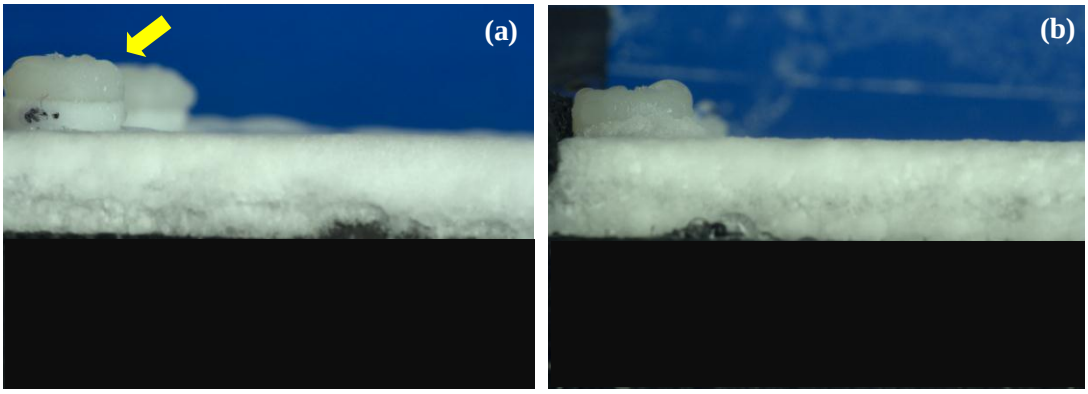

Figure 7: (a) Image of the frost layer on the baseline surface approx. 2.5 hours into the experiment (80% RH, 22.0V) (b) Image of the frost layer on the hydrophobic surface approx. 2.5 hours into the experiment (80% RH, 22.0V)

layer on Sample 2 was "thicker and fluffier" than the frost layer on Sample 1. A few other observations can be made here. First, the difference in frost mass between the two surfaces continued to grow monotonically throughout the experiment whereas the difference in frost thickness between the two surfaces remained fairly constant after the early frost growth period. Second, the density of the baseline surface remained roughly twice the density of the hydrophobic surface throughout the experimental testing period. These findings suggest that beyond the initial condensation period, the frost layer grew at similar rates on both the baseline and hydrophobic surfaces. This further suggests that while hydrophobic surfaces produce slightly thicker frost layers, it may be possible to account for this during the initial design of a heat exchanger. Thus, potential performance enhancements associated with improved defrosting on a hydrophobic surface could ultimately be more important (in certain applications) than the disadvantage associated with the thicker frost layer that forms on these surfaces.

3.2 Defrosting/Cycling Test (CT) Experiments

Cycling tests were also performed as part of this work to evaluate the effectiveness of these surfaces at removing water from the surface during defrosting and the continued ability of the surface to do this following multiple frosting/defrosting events (i.e. cycles) — see Table 4. In this table, the "defrosting percentage" is defined as the ratio of drained water mass to the initial mass of frost on the surface prior to defrosting. Due to small differences in the defrost time for Sample 2, another metric Φ was used to more fairly compare Sample 2 with the other surfaces. This metric takes into account differences in the defrost time as well as differences in the initial frost mass on the surface. This is important since surfaces with a higher initial frost mass might be expected to drain more water due to the higher gravitational forces experienced by the frost layer. As expected, the defrosting percentage and defrost metric Φ displayed similar trends. (Note: Larger Φ means more efficient defrosting.) It should be noted here that in all cases the hydrophobic surface (Sample 2) outperformed the baseline surface (Sample 1) and removed the most water of all the surfaces tested. Moreover, the increase in Φ was persistent and remained nearly constant during all three cycles — i.e. 24-26% higher than the baseline surface. This stands in contrast to Sample 3 which removed more water than the baseline surface during the first defrost cycle but increasingly lost this advantage in subsequent defrost cycles. In fact, in most cases after the third defrost cycle, the defrost efficiency of Sample 3 was comparable to the baseline surface as shown in Table 4.

Table 4: Defrosting Efficiency Data from One Hour Cycling Tests (CT)

No.	Defrosting Efficiency	Sample 1 (Baseline)	Sample 2 (Hydrophobic) *	Sample 3 (Wedge Shape)
1	60% RH, 22.0V Cycle 1	Φ = 5.824	Φ = 7.315	Φ = 6.785
		80.9%	*n/a*	94.2%
2	60% RH, 22.0V Cycle 2	Φ = 5.358	Φ = 6.635	Φ = 5.540
		72.9%	*n/a*	76.9%
3	60% RH, 22.0V Cycle 3	Φ = 6.182	Φ = 7.686	Φ = 6.186
		56.7%	*n/a*	55.0%

Note: Uncertainty: ±3-4% * Defrosting time was slightly different than Samples 1 and 3

Defrosting Metrics

$$\Phi = \frac{(m_{\text{removed}}) \times (t_{\text{frost}})}{(t_{\text{defrost}}) \times (m_{\text{initial}})}$$

where $t_{\text{frost}} = 3600\text{s}$

$$\% = \frac{m_{\text{removed}}}{m_{\text{initial}}}$$

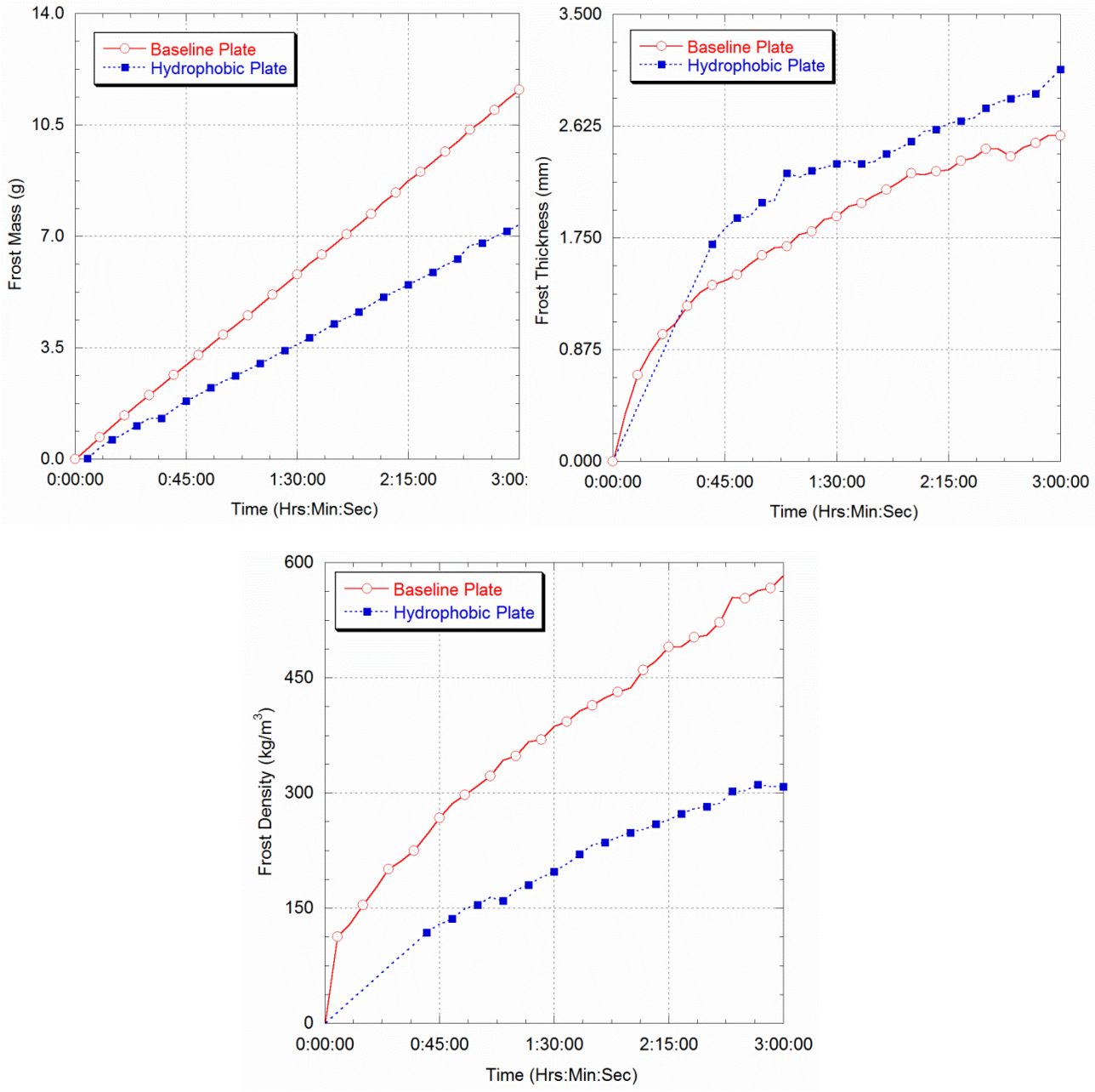

Figure 8: Comparison of frost mass, frost thickness, and frost density on the baseline plate (Sample 1) and the hydrophobic plate (Sample 2) for 18.6V, 80% RH

Additional tests are currently being performed on surfaces containing a wettability pattern and/or a surface tension gradient to help facilitate the movement of water to preferred locations on the heat transfer surface. It is believed that such surfaces could be used to affect the properties of the frost layer (i.e. density, thermal conductivity, etc.) and/or increase water drainage during the defrost cycle. Sample 3 which contained a wedge-shaped gradient was fabricated with this view in mind using the methodology described in Alheshibri et al. (2013). Figure 9 shows how this surface not only affects the distribution of condensate on the surface following the defrost period but also how it can affect the characteristics of the resulting frost layer and its growth. Sample 4 which was constructed using laser-etching techniques contains a radial surface tension gradient that is designed to promote the coalescence of condensate droplets for easier removal via gravity. Tests on these surfaces are currently underway, and the results will be discussed in a future publication.

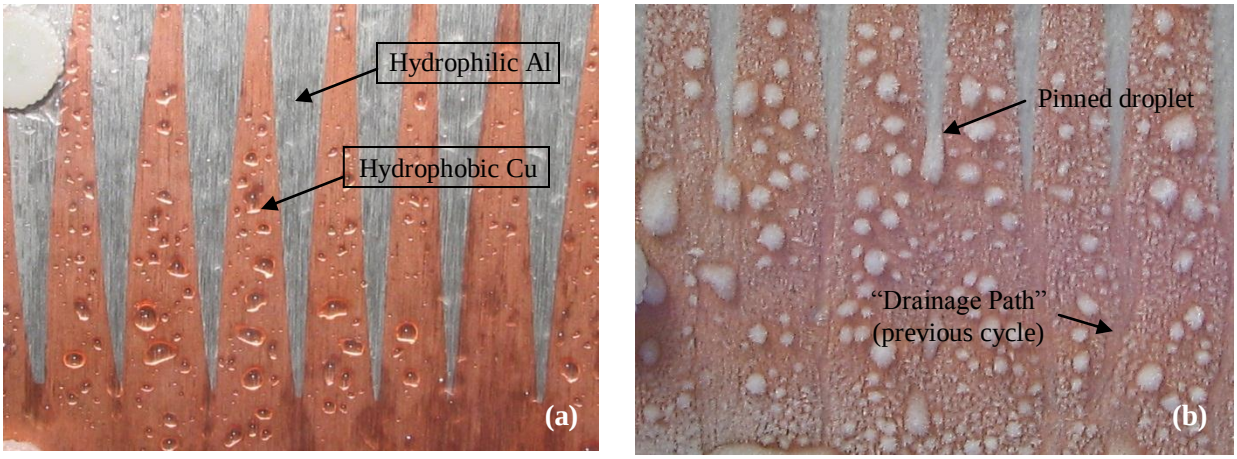

Figure 9: Images of water distribution and frost growth on Sample 3 following a defrost cycle (different experiments)

4. CONCLUSIONS

In this work the properties of a growing frost layer for surfaces of varying wettability were analyzed to determine the effect that the surface energy has on the frost mass, thickness, and density. The experimental methodology was validated using a baseline surface (Sample 1). The results obtained for the frost thickness as a function of the temperature and relative humidity showed good agreement with results reported in the literature.

The effect of surface energy on the frost mass thickness and density was then investigated using the hydrophobic surface (Sample 2). For the normal frost growth experiments, the resultant frost layer for the hydrophobic surface was "thicker and fluffier" resulting in a less dense frost. While the difference in frost mass between the two surfaces continued to grow monotonically throughout the experiment, the difference in frost thickness remained fairly constant after the early frost growth period. Also, the density of the baseline surface remained roughly twice the density of the hydrophobic surface. These results suggest that beyond the initial condensation period, the frost layer grew at similar rates on both the baseline and hydrophobic surfaces. This further suggests that while hydrophobic surfaces produce slightly thicker frost layers, it may be possible to account for this during the initial design of a heat exchanger. Thus, potential performance enhancements associated with improved defrosting on a hydrophobic surface could ultimately be more important (in certain applications) than the disadvantage associated with the thicker frost layer that forms on these surfaces.

Defrost cycling tests showed that the hydrophobic surface (Sample 2) consistently removed more water than the baseline surface (Sample 1) during each of the three consecutive frosting-defrosting events. In contrast, Sample 3 which contained a wettability pattern removed more water than the baseline surface during the first defrost cycle but increasingly lost this advantage in subsequent defrost cycles. Initial results obtained from Sample 3 showed that this surface not only affected the distribution of condensate on the surface following the defrost period, but also affected the characteristics of the resulting frost layer and its growth. Future experiments will examine topographically-modified surfaces as well as surfaces with other types of gradients to compare differences in frost mass, thickness, and density.

NOMENCLATURE

A	Heat transfer area	(m^2)	**Greek Symbols**	
CA	Contact angle	(°)	δ	Frost thickness (mm)
h	Heat transfer coefficient	(W/m^2K)	ρ	Density (kg/m^3)
m	Frost mass	(g)	Φ	Defrosting metric (--)
RH	Relative humidity	(%)	**Subscripts**	
T	Temperature	(°C)	f	Frost
V	Voltage	(V)	s	Surface

REFERENCES

Alheshibri, M.H., Rogers, N.G., Sommers, A.D., Eid, K.F., 2013, Spontaneous movement of water droplets on patterned Cu and Al surfaces with wedge-shaped gradients," *Applied Physics Letters* 102, 174103.

Brian, P.L.T., Reid, R.C., Shah, Y.T., 1970, Frost deposition on cold surfaces, *Ind. Eng. Chem. Fund.* 9(3), pp. 375-380.

Cheng, C.-H., Cheng, Y.-C., 2001, Predictions of frost growth on a cold plate in atmospheric air, *Int. Comm. Heat Mass Transfer* 28(7), pp. 953-962.

Cheng, C.-H., Wu, K.-H., 2003, Observations of early-stage frost formation on a cold plate in atmospheric air flow, *J. Heat Transfer* 125, pp. 95-102.

Hayashi, Y., Auki, A., Adachi, S., Hori, K., 1977, Study of frost properties correlating with frost formation types, *J. Heat Transfer* 99, pp. 239-245.

Hoke, J.L., Georgiadis, J.G., Jacobi, A.M., 2004, "Effect of substrate wettability on frost properties," *J. Thermophysics and Heat Transfer* 18(2), pp. 228-235.

Inaba, H. and S. Imai, 1996, Study on sublimation phenomenon of horizontal frost layer exposed to forced convection air flow and radiant heat, *J. Heat Transfer* 118, pp. 694-701.

Jones, B.W., Parker, J.D., 1975, Frost formation with varying environmental parameters, *J. Heat Transfer* 97, 255-257.

Kulinich, S.A., Farhadi, S., Nose, K., Du, X.W., 2011, Superhydrophobic surfaces: Are they really ice-repellent? *Langmuir* 27(1), pp.25-29.

Lee, K.S., Kim, W.S., Lee, T.H., 1997, A one-dimensional model for frost formation on a cold flat surface, *Int. J. Heat Mass Transfer* 40(18), pp. 4359-4365.

Le Gall, R. and J.M. Grillot, 1997, Modeling of frost growth and densification, *Int. J. Heat Mass Transfer* 40(13), pp. 3177-3187.

Na, B., Webb, R.L., 2004a, New model for frost growth rate, *Int. J. Heat Mass Transfer* 47, pp. 925-936.

Na, B., Webb, R.L., 2004b, Mass transfer on and within a frost layer, *Int. J. Heat Mass Transfer* 47, pp. 899-911.

Ogawa, K., Tanaka, N., and M. Takeshita, 1993, Performance improvement of plate fin-and-tube heat exchangers under frosting conditions, *ASHRAE Transactions* 99(1), pp. 762-771.

Östin, R., Andersson, S., 1991, Frost growth parameters in a forced air stream, *Int. J. Heat Mass Transfer* 34, 1009-1017.

Rite, R.W., Crawford, R.R., 1991, A parametric study of the factors governing the rate of frost accumulation on domestic refrigerator-freezer finned-tube evaporator coils, *ASHRAE Transactions* 97(2), pp. 438-445.

Schneider, H.W., 1978, Equation of the growth rate of frost forming on cooled surfaces, *Int. J. Heat Mass Transfer* 21, pp. 1019-1024.

Senshu, T., Yasuda, H., Oguni, K., Ishibani, K., 1990, Heat pump performance under frosting conditions: Part I- Heat and mass transfer on cross-finned tube heat exchangers under frosting conditions, *ASHRAE Transactions* 96(1).

Sherif, S.A., Raju, S.P., Padki, M.M., Chan, A.B., 1993, A semi-empirical transient method for modeling frost formation on a flat plate, *Int. J. Refrig.* 16(5), pp. 321-329.

Shin, J., Tikhonov, A.V., Kim, C., 2003, Experimental study on frost structure on surfaces with different hydrophilicity: density and thermal conductivity, *J. Heat Transfer* 125, pp. 84-94.

Tao, Y.X., Besant, R.W., and K.S. Rezkallah, 1993, A mathematical model for predicting the densification and growth of frost on a flat plate, *Int. J. Heat Mass Transfer* 36(2), pp. 353-363.

White, J.E. and C.J. Cremers, 1981, Prediction of growth parameters of frost deposits in forced convection, *J. Heat Transfer* 103, pp. 3-6.

Yang, D.K., Lee, K.S., 2004, Dimensionless correlations of frost properties on a cold plate, *Int. J. Refrig.* 27, pp. 89-96.

Yang, D.K., Lee, D.H., Kim, J.S., Lee, K.S., 2004, Modeling of frost behavior on a cold plate, *Proc. of the Int'l Refrig. and Air Conditioning Conference at Purdue*, West Lafayette, IN, July 12-15, Paper No. R121.

Yonko, J.D., Sepsy, S.F., 1967, An investigation of the thermal conductivity of frost while forming on a flat horizontal plate, *ASHRAE Transactions* 73(2), pp.1.1-1.11.

Yun, R., Kim, Y., and M. Min, 2002, Modeling of frost growth and frost properties with airflow over a flat plate, *Int. J. Refrig.* 25(3), pp. 362-371

ACKNOWLEDGEMENT

The authors gratefully acknowledge the involvement of others on this project, especially Jeffrey Phillip at Miami University for his help and assistance with some of the data collection during the early stages of this project.